Biogeosciences

Nitrogen cycling in shallow low-oxygen coastal waters off Peru from nitrite and nitrate nitrogen and oxygen isotopes

Happy Hu[1,*], Annie Bourbonnais[1,*], Jennifer Larkum[1], Hermann W. Bange[2], and Mark A. Altabet[1]

[1]School for Marine Science and Technology, University of Massachusetts Dartmouth, 706 South Rodney French Blvd, New Bedford, MA 02744-1221, USA
[2]GEOMAR Helmholtz Centre for Ocean Research Kiel, Düsternbrooker Weg 20, 24105 Kiel, Germany
[*]These authors contributed equally to this work.

Correspondence to: Annie Bourbonnais (abourbonnais@umassd.edu)

Abstract. O_2 deficient zones (ODZs) of the world's oceans are important locations for microbial dissimilatory nitrate (NO_3^-) reduction and subsequent loss of combined nitrogen (N) to biogenic N_2 gas. ODZs are generally coupled to regions of high productivity leading to high rates of N-loss as found in the coastal upwelling region off Peru. Stable N and O isotope ratios can be used as natural tracers of ODZ N-cycling because of distinct kinetic isotope effects associated with microbially mediated N-cycle transformations. Here we present NO_3^- and nitrite (NO_2^-) stable isotope data from the nearshore upwelling region off Callao, Peru. Subsurface oxygen was generally depleted below about 30 m depth with concentrations less than 10 μM, while NO_2^- concentrations were high, ranging from 6 to 10 μM, and NO_3^- was in places strongly depleted to near 0 μM. We observed for the first time a positive linear relationship between NO_2^- $\delta^{15}N$ and $\delta^{18}O$ at our coastal stations, analogous to that of NO_3^- N and O isotopes during NO_3^- uptake and dissimilatory reduction. This relationship is likely the result of rapid NO_2^- turnover due to higher organic matter flux in these coastal upwelling waters. No such relationship was observed at offshore stations where slower turnover of NO_2^- facilitates dominance of isotope exchange with water. We also evaluate the overall isotope fractionation effect for N-loss in this system using several approaches that vary in their underlying assumptions. While there are differences in apparent fractionation factor (ε) for N-loss as calculated from the $\delta^{15}N$ of NO_3^-, dissolved inorganic N, or biogenic N_2, values for ε are generally much lower than previously reported, reaching as low as 6.5 ‰. A possible explanation is the influence of sedimentary N-loss at our inshore stations which incurs highly suppressed isotope fractionation.

1 Introduction

Chemically combined nitrogen (N), e.g., nitrate (NO_3^-), is an important phytoplankton nutrient limiting primary productivity and carbon export throughout much of the ocean (e.g. Gruber, 2008). The marine nitrogen cycle involves a series of microbial processes, which transfer N between a number of chemical forms. These include N_2 fixation, nitrification (ammonium (NH_4^+) and nitrite (NO_2^-) oxidation), and loss of combined N to N_2 via denitrification and anaerobic ammonium oxidation (anammox). Of particular importance is the global balance between sources of combined N (N_2 fixation) and N-loss processes which ultimately control the combined N content of the ocean and thus its productivity and strength of the biological carbon pump. N-loss typically occurs under nearly anoxic conditions where the first step, dissimilatory NO_3^- reduction to NO_2^-, active at oxygen (O_2) concentrations less than ∼ 25 μM (Kalvelage et al., 2011), is used by heterotrophic microbes in lieu of O_2 for respiration. Canonically, the denitrification pathway of successive reduction of NO_3^-, NO_2^-, nitric oxide (NO), and nitrous oxide (N_2O) to N_2 was considered as the dominant pathway for N-loss. However, since the early 2000s, anammox (NO_2^- + NH_4^+ → N_2) was found to be widespread in the ocean (Kuypers et al., 2003, 2005; Hamersley et al., 2007; Dalsgaard et al., 2012; Kalvelage et al., 2013). While it is still a

matter of debate whether denitrification or anammox is the dominant pathways for N-loss in Oxygen Minimum Zones (ODZs) (e.g., Lam et al., 2009; Ward et al., 2009), both N-loss processes have been shown to strongly vary spatially and temporally and are linked to organic matter export and composition (Kalvelage et al., 2013; Babbin et al., 2014). It follows that there is still considerable uncertainty as to the controls on N-loss as well as the role for other linking processes such as DNRA (NO_3^- to NH_4^+) and NO_2^- oxidation in the absence of O_2.

Marine N-loss to N_2 occurs predominately in reducing sediments and the O_2 deficient water columns found in the Arabian Sea and Eastern Tropical North and South Pacific ODZs (Lam and Kuypers, 2011 and references therein; Ulloa et al., 2012). NO_2^- is an important intermediate during N-loss and generally accumulates at concentrations up to $\sim 10\,\mu M$ in these regions (Codispoti et al., 1986; Casciotti et al., 2013). The depletion of NO_3^- is typically quantified as a dissolved inorganic N (DIN $= NO_3^- + NO_2^- + NH_4^+$) deficit relative to phosphate (PO_4^{-3}) assuming Redfield stoichiometry and the accumulation of biogenic N_2 (when measured) is detected as anomalies in N_2 / Ar relative to saturation with atmosphere (Richards and Benson, 1961; Chang et al., 2010; Bourbonnais et al., 2015).

NO_3^- and NO_2^- N and O isotopes represent a useful tool to study N cycle transformations as they respond to in situ processes and integrate over their characteristic time and space scales. Biologically mediated reactions are generally faster for lighter isotopes. For instance, both NO_3^- uptake and dissimilatory NO_3^- reduction produce a strong enrichment in both ^{15}N ($\delta^{15}N = [(^{15}N / ^{14}N_{sample}) / (^{15}N / ^{14}N_{standard}) - 1] \times 1000$) and ^{18}O ($\delta^{18}O = [(^{18}O / ^{16}O_{sample}) / (^{18}O / ^{16}O_{standard}) - 1] \times 1000$) in the residual NO_3^- (Cline and Kaplan, 1975; Brandes et al., 1998; Voss et al., 2001; Granger et al., 2004, 2008; Sigman et al., 2005).

Canonical values for the N isotope effect ($\varepsilon \approx \delta^{15}N_{substrate} - \delta^{15}N_{product}$, without significant substrate depletion) associated with microbial NO_3^- reduction during water column denitrification range from 20 to 30‰ (Brandes et al., 1998; Voss et al., 2001; Granger et al., 2008). In contrast, the expression of the isotope effect of sedimentary denitrification is highly suppressed as compared to the water-column (generally < 3‰) mostly due to near complete consumption of the porewater NO_3^- and diffusion limitation (Brandes and Devol, 1997; Lehmann et al., 2007; Alkhatib et al., 2012). The $\delta^{15}N$ and $\delta^{18}O$ of NO_3^- are affected in fundamentally different ways during NO_3^- consumption and production processes. The ratio of the ^{15}N and ^{18}O fractionation factors ($^{18}\varepsilon : ^{15}\varepsilon$) during NO_3^- consumption during denitrification or assimilation by phytoplankton in surface waters is close to 1 : 1 (Casciotti et al., 2002; Granger et al., 2004, 2008). While the $\delta^{15}N$ of the newly nitrified NO_3^- depends on the $\delta^{15}N$ of the precursor molecule being

nitrified, the O atom is mostly derived from water (with a $\delta^{18}O$ of ~ 0‰) with significant isotopic fractionation associated with O incorporation during NO_2^- and NH_4^+ oxidation (Casciotti, 2002; Buchwald and Casciotti, 2010; Casciotti et al., 2010). Therefore, any deviation from this 1:1 ratio in the field has been interpreted as evidence that NO_3^- regeneration is co-occurring with NO_3^- consumption (Sigman et al., 2005; Casciotti and McIlvin, 2007; Bourbonnais et al., 2009). NO_2^- oxidation is associated with an inverse N isotope effect (Casciotti, 2009), atypical of biogeochemical reactions, and can cause both lower and higher ratios for $^{18}\varepsilon : ^{15}\varepsilon$ compared to pure NO_3^- assimilation or denitrification, depending on the initial isotopic compositions of the NO_2^- and NO_3^- and the ^{18}O added back (Casciotti et al., 2013).

Additional information on N-cycling processes can be obtained from the isotopic composition of NO_2^-. For example, because of its inverse N isotope effect, NO_2^- oxidation results in a lower NO_2^- $\delta^{15}N$ than initially produced by NH_4^+ oxidation and NO_3^- reduction (Casciotti, 2009; Brunner et al., 2013). Logically, NO_2^- reduction would be expected to produce a positive relationship between $\delta^{15}N$-NO_2^- and $\delta^{18}O$-NO_2^- though there are no quantitative observations in the literature. Analogous to NO_3^- reduction, it also involves enzymatic breakage of the N-O bond. However, O-isotope exchange of NO_2^- with water (as a function of pH and temperature) would reduce the slope of a NO_2^- $\delta^{18}O$ vs. $\delta^{15}N$ relationship toward zero. NO_2^- turnover time can therefore be assessed from this observed relationship and in situ pH and temperature (Buchwald and Casciotti, 2013).

It is still under discussion whether the global ocean N budget is in balance. Current estimates from direct observations and models for N_2 fixation, considered the primary marine N source, range from 110–330 Tg N yr^{-1} (Brandes and Devol, 2002; Gruber, 2004; Deutsch et al., 2007; Eugster and Gruber, 2012; Großkopf et al., 2012). Estimates for major marine N-sinks, i.e., denitrification and anammox in the water-column of oxygen deficient zones and sediments account for 145–450 Tg N yr^{-1} (Gruber, 2004; Codispoti, 2007; DeVries et al., 2012; Eugster and Gruber, 2012). Large uncertainties are associated with this budget, mainly in constraining the proportion of sedimentary denitrification which is typically estimated from ocean's N isotope balance and the expressed isotope effects for water-column vs. sedimentary NO_3^- reduction during denitrification (e.g. Brandes and Devol, 2002; Altabet, 2007; DeVries et al., 2012). Liu (1979) was first to suggest a lower ε for denitrification in the Peru ODZ as compared to the subsequently accepted canonical range for NO_3^- reduction of 20 to 30‰ (Brandes et al., 1998; Voss et al., 2001; Granger et al., 2008). Ryabenko et al. (2012) provided a more widely distributed set of data in support. Most recently, a detailed study in a region of extreme N-loss associated with a Peru coastal mode-water eddy confirmed an ε value for N-loss of ~ 14‰ (Bourbonnais et al., 2015). Ap-

plying such a lowered value to global budgets would bring the global N budget closer to balance.

Ryabenko et al. (2012) also suggested that ε values were even lower in the shelf region of the Peru ODZ. To investigate further, we present here N and O isotope data for NO_2^- and NO_3^- from shallow coastal waters near Callao, off the coast of Peru. These waters are highly productive as a consequence of active upwelling that is also responsible for shoaling of the oxycline. We determine the relationship between NO_2^- $\delta^{15}N$ and $\delta^{18}O$ and its implication for NO_2^- cycling in these shallow waters as compared to offshore stations. We finally derive isotope effects for N-loss and infer the likely influence of sedimentary N-loss, which incurs a highly suppressed isotope effect, at our relatively shallow sites.

2 Material and methods

2.1 Sampling

The R/V *Meteor 91* research cruise (M91) to the eastern tropical South Pacific Ocean off Peru in December 2012 was part of the SOPRAN program and the German SFB 754 project. It included an along shore transect of seven inner shelf stations located between 12 to 14° S that were chosen for this study (Fig. 1). These stations had a maximum depth of 150 m except for station 68 (250 m depth). We additionally sampled deep offshore stations during the M90 cruise in November 2012. Samples for NO_3^- and NO_2^- isotopic composition and N_2 / Ar ratio were collected using Niskin bottles mounted on a CTD/Rosette system, which was equipped with pressure, temperature, conductivity, and oxygen sensors. O_2 concentrations were determined using a Seabird sensor, calibrated using the Winkler method (precision of $0.45\,\mu mol\,L^{-1}$) with a lower detection limit of $2\,\mu mol\,L^{-1}$. Nutrients concentrations were measured on board using standard methods as described in Stramma et al. (2013).

2.2 NO_2^- and NO_3^- isotope analysis

NO_2^- samples were stored in 125 mL HDPE bottles preloaded with 2.25 mL 6 M NaOH to prevent microbial activity as well as alteration of $\delta^{18}O$-NO_2^- by isotope exchange with water (Casciotti et al., 2007). Bottles were kept frozen after sample collection, though we have subsequently determined in the laboratory that seawater samples preserved in this way can be kept at room temperature for at least a year without alteration of NO_2^- $\delta^{15}N$ or $\delta^{18}O$ (unpublished data). Samples were analyzed by continuous He flow isotope-ratio mass spectrometry (CF-IRMS; see below) after chemical conversion to N_2O using acetic acid buffered sodium azide (McIlvin and Altabet, 2005). Because of high sample pH, the reagent was modified for NO_2^- isotope analysis by increasing the acetic acid concentration to 7.84 M. In-house (i.e., MAA1, $\delta^{15}N = -60.6\,‰$;

MAA2, $\delta^{15}N = 3.9\,‰$; Zh1, $\delta^{15}N = -16.4\,\%$) and other laboratory calibration standards (N23, $\delta^{15}N = 3.7\,‰$ and $\delta^{18}O = 11.4\,‰$; N7373, $\delta^{15}N = -79.6\,‰$ and $\delta^{18}O = 4.5\,‰$; and N10219; $\delta^{15}N = 2.8\,‰$ and $\delta^{18}O = 88.5\%$; see Casciotti and McIlvin, 2007) were used for NO_2^- $\delta^{15}N$ and $\delta^{18}O$ analysis.

NO_3^- samples were stored in 125 mL HDPE bottles preloaded with 1 mL of 2.5 mM sulfamic acid in 25 % HCl to both act as a preservative and to remove NO_2^- (Granger and Sigman, 2009). Samples were also kept at room temperature and we have found that they can be stored in this way for many years without alteration of NO_3^- $\delta^{15}N$ or $\delta^{18}O$. Cadmium reduction was used to convert NO_3^- to NO_2^- prior to conversion to N_2O using the "azide method" (McIlvin and Altabet, 2005) and IRMS analysis. Standards for NO_3^- isotope analysis were N3 ($\delta^{15}N = 4.7\,‰$ and $\delta^{18}O = 25.6\,‰$), USGS34 ($\delta^{15}N = -1.8\,‰$ and $\delta^{18}O = -27.9\,‰$), and USGS35 ($\delta^{15}N = 2.7\,‰$ and $\delta^{18}O = 57.5\,‰$) (Casciotti et al., 2007). The lowest concentration of NO_2^- or NO_3^- analyzed for isotopic composition was $0.5\,\mu M$, thus $\delta^{15}N$-NO_3^- and $\delta^{15}N$-NO_2^- could not be measured below 37 m at station 63.

A GV Instruments IsoPrime Isotope Ratio Mass Spectrometer (IRMS) coupled to an on-line He continuous-flow purge and/or trap preparation system was used for isotope analysis (Sigman et al., 2001; Casciotti et al., 2002; McIlvin and Altabet, 2005). N_2O produced by the azide reaction was purged with He from the septum sealed 20 mL vials and trapped, cryofocused and purified prior to transfer to the IRMS. Total run time was $700\,s\,sample^{-1}$ (McIlvin and Altabet, 2005). Isotopic values are referenced against atmospheric N_2 for $\delta^{15}N$ and VSMOW for $\delta^{18}O$. Reproducibility was 0.2 and 0.5 ‰, respectively.

2.3 N_2 / Ar IRMS analysis and calculation of biogenic N_2 and $\delta^{15}N$ biogenic N_2

The accumulation of biogenic N_2 from denitrification and anammox can be measured directly from precise N_2 / Ar measurements (see above; Richards and Benson, 1961; Chang et al., 2010; Bourbonnais et al., 2015). As described in Charoenpong et al. (2014), N_2 / Ar samples were collected from Niskin bottles using 125 mL serum bottles, and all samples were treated with $HgCl_2$ as a preservative and filled without headspace. When cavitation bubbles formed from cooling of warm, near-surface samples, these bubbles were collapsed and reabsorbed by warming samples in the laboratory in a 30–35 °C water bath before analysis. N_2 / Ar was measured using an automated dissolved gas extraction system coupled to a multicollector IRMS (Charoenpong et al., 2014). Excess N_2 was calculated first from anomalies relative to N_2 / Ar expected at saturation with atmosphere at in situ temperature and salinity. Locally produced biogenic N_2 was obtained by subtracting excess N_2 at the corresponding density surface for waters outside of the ODZ ($O_2 > 10\,\mu M$)
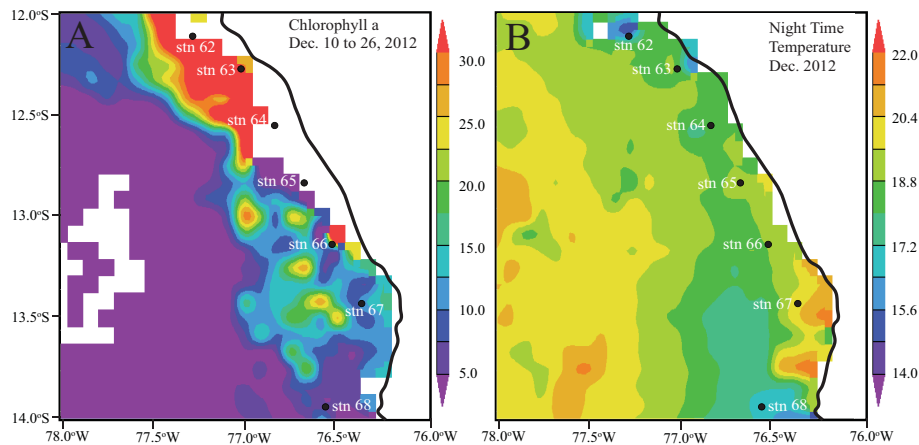
Figure 1. Station map with satellite data from http://disc.sci.gsfc.nasa.gov/giovanni/. **(a)** sea surface chlorophyll a concentrations ($\mathrm{mg\,m^{-3}}$), **(b)** nighttime sea surface temperature ($^\circ$C).

not affected by N-loss (Chang et al., 2010; Bourbonnais et al., 2015). δ^{15}N biogenic N_2 was calculated from the δ^{15}N-N_2 anomaly as in Bourbonnais et al. (2015). Reproducibility was better than $0.7\,\mu$M for excess N_2 and 0.03 ‰ for δ^{15}N-N_2. δ^{15}N of biogenic N_2 was calculated by mass balance as in Bourbonnais et al. (2015).

2.4 Isotope effect (ε) calculations

Isotope effects are estimated using the Rayleigh equations describing the change in isotope ratio as a function of fraction of remaining substrate. The following equations are used for a closed system (Mariotti et al., 1981):

$$\delta^{15}\mathrm{N-NO_3^-} = \delta^{15}\mathrm{N-NO_3^-}\,(f=1) - \varepsilon \times \ln[f_1] \text{ or} \quad (1)$$

$$\delta^{15}\mathrm{N-DIN} = \delta^{15}\mathrm{N-DIN}(f=1) - \varepsilon \times \ln[f_2], \quad (2)$$

where f_1 is the fraction of remaining $\mathrm{NO_3^-}$ and f_2 is the fraction of remaining DIN ($\mathrm{NO_3^-}+\mathrm{NO_2^-}$ concentrations). δ^{15}N-DIN is the average δ^{15}N for $\mathrm{NO_3^-}$ and $\mathrm{NO_2^-}$ weighted by their concentrations. The fraction of remaining DIN is a better estimation of the overall effective isotope effect for N-loss (Bourbonnais et al., 2015), while using $\mathrm{NO_3^-}$ as the basis to calculate ε specifically targets $\mathrm{NO_3^-}$ reduction. See below for details of f value calculation.

The overall isotope effect for N-loss can also be estimated from the δ^{15}N of biogenic N_2 produced:

$$\delta^{15}\mathrm{N-biogenic\ N_2} = \delta^{15}\mathrm{N\text{-}DIN}(f=1) \\ + \varepsilon \times f_2/[1-f_2] \times \ln[f_2], \quad (3)$$

whereas the closed system equations assume no addition or loss of substrate or product, corresponding steady-state open system equations can account for such effects (Altabet,

2005):

$$\delta^{15}\mathrm{N-NO_3^-} = \delta^{15}\mathrm{N-NO_3^-}\,(f=1) + \varepsilon[1-f_1] \text{ or} \quad (4)$$

$$\delta^{15}\mathrm{N-DIN} = \delta^{15}\mathrm{N-DIN}(f=1) + \varepsilon \times [1-f_2] \quad (5)$$

$$\delta^{15}\mathrm{N-biogenic\ N_2} = \delta^{15}\mathrm{N-DIN}(f=1) - \varepsilon \times f_2. \quad (6)$$

For all equations, the slope represents ε and the y intercept is the initial δ^{15}N prior to N-loss. For calculations using Eqs. (3) and (6) we only used δ^{15}N values associated with biogenic N_2 greater than $7.5\,\mu$M because of increasing noise below this level due to the large atmospheric dissolved N_2 background (typically up to $\sim 500\,\mu$M).

Since the closed system equations assume no loss or re-supply of substrate or production in a water parcel, they are appropriate where there is little mixing and/or advection is dominant over mixing. The open system equations take into account supply from or loss to surrounding water parcels, e.g. mixing dominance. Both cases represent extreme situations. In the next section, we will estimate and compare ε using both sets of equations.

To do so, we need to estimate the fraction of $\mathrm{NO_3^-}$ or DIN remaining (f). The assumption of Redfield stoichiometry (as in Eq. 9) in source waters is typically made:

$$f_{1p} = [\mathrm{NO_3^-}]/\mathrm{Np_{expected}} \text{ or} \quad (7)$$

$$f_{2p} = ([\mathrm{NO_3^-}]+[\mathrm{NO_2^-}])/\mathrm{Np_{expected}} \quad (8)$$

$$\mathrm{Np_{expected}} = 15.8 \cdot ([\mathrm{PO_4^{3-}}] - 0.3) \quad (9)$$

$$\mathrm{N_{observed}} = [\mathrm{NO_3^-}]+[\mathrm{NO_2^-}]+[\mathrm{NH_4^+}], \quad (10)$$

where $\mathrm{Np_{expected}}$ is the concentration expected assuming Redfield stoichiometry. Equation (9) was derived in Chang et al. (2010) from stations to the west of the ETSP ODZ (143–146° W) and takes into account preformed nutrient concentrations. In our study, $\mathrm{NH_4^+}$ generally did not significantly accumulate, except at station 63, and was thus not included.

This has been the traditional approach to quantify N-loss in ODZs (N deficit, Np_{def}), by comparing observed DIN concentrations ($N_{observed}$) to $Np_{expected}$:

$$Np_{def} = Np_{expected} - N_{observed}. \tag{11}$$

However, the assumption of Redfield stoichiometry may not be appropriate in this shallow environment due to preferential release of PO_4^{3-} following iron and manganese oxyhydroxide dissolution in anoxic sediments (e.g., Noffke et al., 2012). An alternative method of calculating f makes use of our biogenic N_2 measurements to estimate expected N prior to N-loss ($N_{expected}$–bio N_2) and f values based on it:

$$N_{expected} - bio\ N_2 = [NO_3^-] + [NO_2^-] + 2 \times [Biogenic\ N_2] \tag{12}$$

$$f_{1bioN_2} = [NO_3^-]/N_{expected} - bioN_2 \ or \tag{13}$$

$$f_{2bioN_2} = [NO_3^- + NO_2^-]/N_{expected} - bio\ N_2. \tag{14}$$

A third way to estimate f is to use NO_3^- or DIN concentrations divided by observed maximum NO_3^- or DIN concentrations for the source of the upwelled waters (see red rectangles in Fig. 2).

3 Results

3.1 Hydrographic characterization

During the study period, there was active coastal upwelling especially at station 63 as seen by relatively low satellite sea surface temperatures, higher chlorophyll a concentrations, and a shallow oxycline (Fig. 1). A common relationship and narrow range for T and S were found, comparable to T / S signatures for offshore ODZ waters between ~ 100 and 200 m depths (Bourbonnais et al. 2015), indicating a common source of water upwelling at these inner shelf stations (Fig. 2). This is expected in these shallow waters, where upwelling of the Peru coastal current with low O_2 and high nutrients plays a dominant role (Penven et al., 2005). O_2 increased only in warmer near-surface waters as a consequence of atmospheric exchange. There was a change in surface water temperature from 15 to 20 °C (Fig. 1b) with distance along the coast (from 12.0 to 14.0° S, about 222 km) that indicates corresponding changes in upwelling intensity. Stronger local wind forcing likely brought up colder deep water near station 63.

3.2 Dissolved O_2 and nutrient concentrations

As a consequence of active upwelling sourced from the offshore ODZ, the oxycline was very shallow at our inshore stations. O_2 was generally depleted below 10 to 20 m (Fig. 3a) and was always less than 10 μM below 30 m. Because we are focusing on N-transformations that occur in the absence of O_2, our data analyses will be mainly restricted to samples where O_2 concentration is below this value. Whereas a recent study indicates that denitrification and anammox are reversibly suppressed at nanomolar O_2 levels (Dalsgaard et al., 2014), CTD deployed Seabird O_2 sensors are not sufficiently sensitive to detect such low concentrations and hence our choice of a 10 μM threshold. In contrast, NO_2^- oxidation, an aerobic process, was shown to occur even at low to non-detectable O_2 (Füssel et al., 2012).

Both $Si(OH)_4$ and PO_4^{3-} concentrations had very similar vertical and along section distributions (Fig. 3c, d). Concentrations were at a minimum at the surface, presumably due to phytoplankton uptake, and increased with depth to up to 46 and 3.7 μM, respectively. Station 63 had the highest near-bottom concentrations, a likely result of release from the sediments, which is futher supported by high near-bottom NH_4^+ concentrations (up to ~ 4 μM) as compared to the other stations (Fig. 3b, c, d).

In contrast to other nutrients, NO_3^- and NO_2^- concentrations were lowest near-bottom at station 63, only reaching their maxima above 60 m. Across most of our stations, NO_3^- concentration was 22 μM at 20 to 40 m depth but decreased to near zero deeper within the O_2-depleted zone due to microbially mediated NO_3^- reduction (Fig. 4a). NO_2^- concentrations correspondingly ranged from 6 to 11 μM for O_2 concentrations less than 10 μM (Fig. 4b). The highest NO_2^- concentration (11 μM) was found at around 50 m (station 64), but only reached 6 μM at all other stations.

3.3 NO_2^- and NO_3^- isotope compositions

As a consequence of kinetic isotope fractionation during N-loss, the N and O isotope composition of NO_3^- and NO_2^- varied inversely with NO_3^- and NO_2^- concentrations, with maximum $\delta^{15}N$ and $\delta^{18}O$ values near the bottom at each station. $\delta^{15}N$-NO_3^- increased from about 10 ‰ in surface waters to up to 50 ‰ in the O_2-depleted zone (Fig. 4c), with near bottom values at station 64 significantly higher (50 ‰) than at the other stations which ranged from 20 to 30 ‰ . $\delta^{15}N$-NO_2^- varied from −25 to about 10 ‰ (Fig. 4d), with maximum values also in deeper waters at station 64.

As expected for NO_3^- reduction, $\delta^{18}O$-NO_3^- positively covaried with $\delta^{15}N$-NO_3^- and ranged from 12 to 46 ‰. We observed an overall linear relationship between $\delta^{15}N$-NO_3^- and $\delta^{18}O$-NO_3^- with a slope of 0.86, which was significantly different than 1 (p value < 0.05), and a y intercept of 1.90 ($r^2 = 0.996$, see Fig. 5a). NO_3^- $\delta^{15}N$ and $\delta^{18}O$ have been shown to increase equally (ratio 1 : 1) during assimilatory and dissimilatory NO_3^- reduction (Casciotti et al., 2002; Granger et al., 2004, 2008). However, deviations from this trend have been observed in the ocean and interpreted as evidence for co-occurring NO_3^- production processes (Sigman et al., 2005; Casciotti and McIlvin, 2007; Bourbonnais et al., 2009, 2015). In this study, we observed a NO_3^- $\delta^{18}O$ vs. $\delta^{15}N$
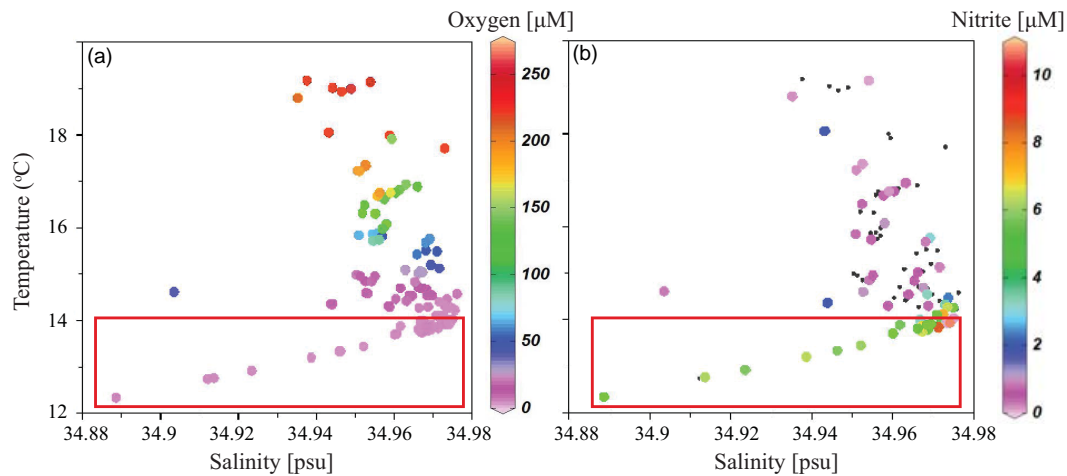
Figure 2. Temperature vs. salinity plots. In **(a)**, color indicates O_2 concentration (μM). In **(a)**, color indicates NO_2^- concentration (μM). Black dots in **(b)** mean no NO_2^- concentration data are available. Points in red rectangle at bottom of each plot belong to station 68 for depths greater than 150 m.
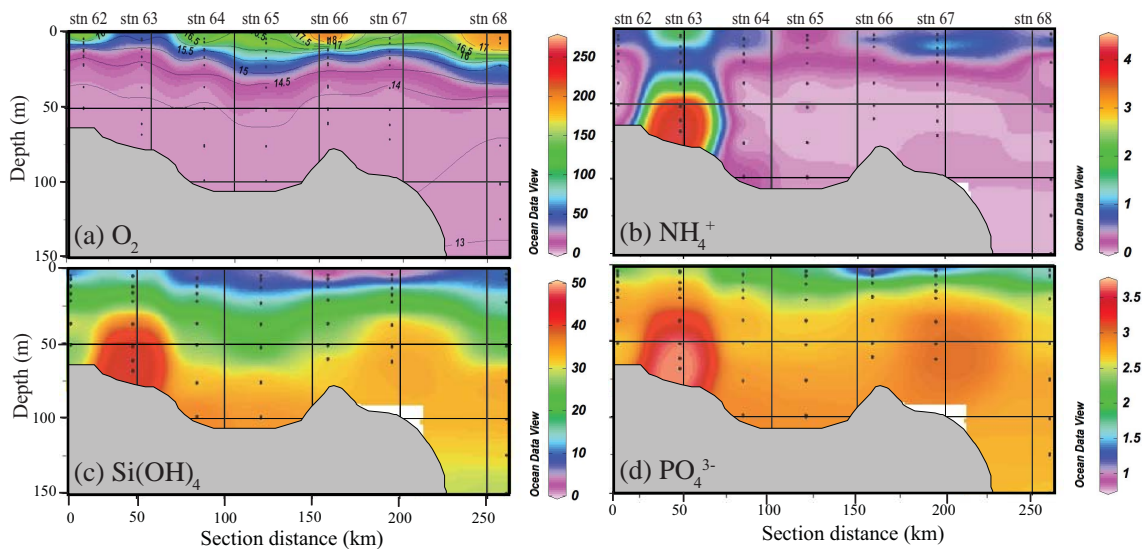

Figure 3. O_2 and nutrient distribution along the transect. **(a)** O_2 concentration (μM) with isotherm overlay, **(b)** NH_4^+ concentration (μM), **(c)** $Si(OH)_4$ concentration (μM) and **(d)** PO_4^{3-} concentration (μM). Grey region represents bathymetry. The depth for station 68 is 253 m.

relationship less than 1, likely originating from NO_2^- re-oxidation to NO_3^- in our environmental setting as in Casciotti and McIlvin (2007). We also observed, for the first time, a significant correlation between $\delta^{15}N$-NO_2^- and $\delta^{18}O$-NO_2^- in the ODZ for our in-shore water stations (Fig. 5b). As in prior studies (Casciotti and McIlvin, 2007; Casciotti et al., 2013), no such relationship was observed by us for a nearby set of offshore stations (see Fig. 5c) where longer NO_2^- turnover times likely facilitated O isotope exchange with water. We will discuss implications of this unique finding in the next section.

3.4 The $\delta^{15}N$ difference between NO_3^- and NO_2^-

The difference in $\delta^{15}N$ between NO_3^- and NO_2^- ($\Delta\delta^{15}N$) reflects the combined isotope effects of simultaneous NO_3^- reduction, NO_2^- reduction, and NO_2^- oxidation. For NO_3^- reduction alone, highest $\Delta\delta^{15}N$ values would be around 25 ‰ at steady-state (Cline and Kaplan, 1975; Brandes et al., 1998; Voss et al., 2001; Granger et al., 2004, 2008). The effect of NO_2^- reduction would be to increase the $\delta^{15}N$ of the residual NO_2^-, thus decreasing $\Delta\delta^{15}N$. In contrast, NO_2^- oxidation is associated with an inverse kinetic isotope effect (Casciotti, 2009) which acts to decrease the residual $\delta^{15}N$ of NO_2^-
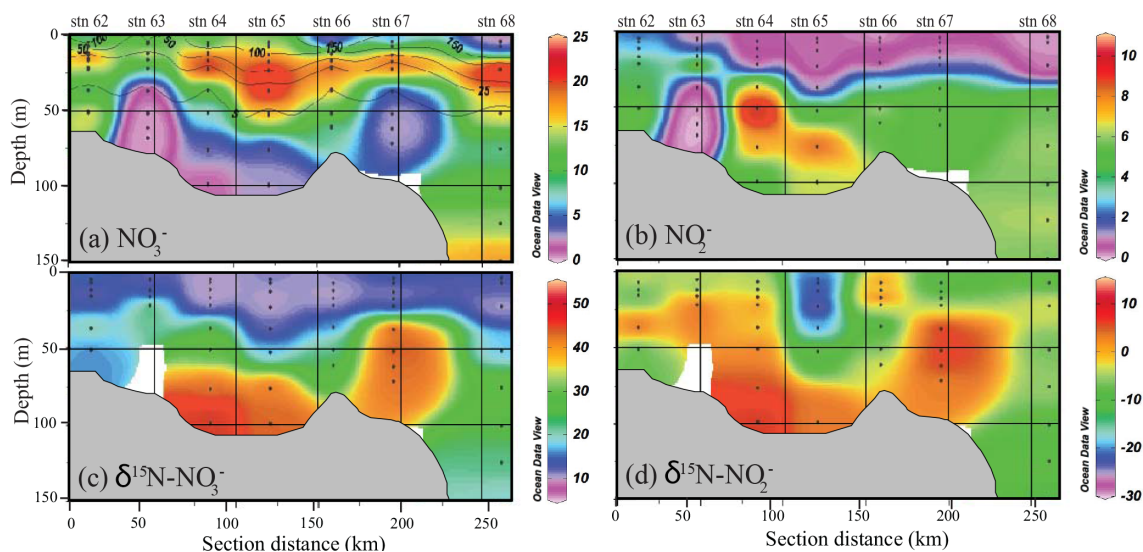
Figure 4. Transects off the Peru coast for **(a)** NO_3^- concentration (µM) with O_2 overlay, **(b)** NO_2^- concentration (µM), **(c)** $\delta^{15}N\text{-}NO_3^-$ (‰) and **(d)** $\delta^{15}N\text{-}NO_2^-$ (‰). Gray region represents approximate bathymetry. No isotopic data are available for the deeper samples collected at station 63, because NO_3^- and NO_2^- concentrations were below analytical limits (< 0.5 µM).

and hence overall increases the $\Delta\delta^{15}N$. Therefore, following NO_2^- oxidation, $\Delta\delta^{15}N$ may be larger than expected from NO_3^- and NO_2^- reduction alone, especially if the system is not at steady-state (Casciotti et al., 2013). $\Delta\delta^{15}N$ ranged from 15 to 40 ‰ (average $= 29.78$ ‰ and median $= 32.5$ ‰) for samples with $O_2 < 10$ µM. These results confirm the presence of NO_2^- oxidation for at least some of our depth intervals.

3.5 N deficit, biogenic N_2 and $\delta^{15}N\text{-}N_2$

N deficits, biogenic N_2 concentrations, and $\delta^{15}N\text{-}N_2$ anomalies relative to equilibrium with atmosphere were overall greater in the O_2-depleted zone reaching highest values near the bottom of station 63 (Fig. 7). N deficit, calculated assuming Redfield stoichiometry (Eqs. 9 to 11), ranged from 17 to 59 µM in this region. The concentration of biogenic N in N_2 ranged from 12 to 36 µM-N and, as expected, was strongly linearly correlated with N deficit ($r^2 = 0.87$; Fig. 8c). However, the slope of 0.45 for the linear relationship shows biogenic N in N_2 to be only half that expected from Np_{def}, a possible consequence of benthic PO_4^{3-} release. The linear relationship ($r^2 = 0.91$) observed between biogenic N in N_2 and DIN (Fig. 8a) supports a single initial DIN value for the source waters to our stations and hence validates using this as a basis for calculating f. The slope of the correlation (0.74) is much closer to 1 as compared to the correlation with Np_{def}, further supporting excess PO_4^{-3} as a contributor to the latter. However this value is still significantly less than 1, suggesting that biogenic N in N_2 may also be underestimated. Because our data are restricted to O_2-depleted depths, it is unlikely that biogenic N_2 was lost to the atmosphere. Al-

ternatively, mixing of water varying in N_2 / Ar can result in such underestimates of biogenic N_2 when N_2 / Ar anomalies are used to calculate excess N_2 (see Charoenpong et al., 2014). As seen below, our estimates of ε are rather insensitive to choice of Np_{def}, biogenic N in N_2, or DIN concentration changes as the basis for calculation of f.

The $\delta^{15}N\text{-}N_2$ anomaly, i.e., the difference between the $\delta^{15}N\text{-}N_2$ observed and at equilibrium, derived as in Charoenpong et al. (2014), ranged from -0.2 to 0.1 ‰ (Fig. 7c). The corresponding range in $\delta^{15}N$ biogenic N_2 at $O_2 < 10$ µM was from -9.0 to 3.2 ‰. Negative $\delta^{15}N\text{-}N_2$ anomaly (i.e., lower $\delta^{15}N$-biogenic N_2) is produced at the onset of N-loss, because extremely depleted $^{15}N\text{-}N_2$ is first produced. At a more advanced N-loss stage, we expect $\delta^{15}N\text{-}N_2$ anomaly and $\delta^{15}N$-biogenic N_2 to increase, which we observed in this study, as heavier ^{15}N is added to the biogenic N_2 pool. The $\delta^{15}N\text{-}N_2$ anomaly signal appears small when compared to the isotopic composition of NO_3^- and NO_2^- but is (1) analytically significant and (2) the result of dilution by the large background of atmospheric N_2 (400 to 500 µM N_2).

3.6 Isotope effect (ε)

Isotope effects were calculated using Eqs. (1) to (6) to compare closed vs. open system assumptions as well as different approaches to estimating f. Examples of plots of the closed system equations with f calculated using biogenic N_2, are shown in Fig. 6. Comparison of results using all three approaches for calculating f (i.e. Redfield stoichiometry, biogenic N_2 and observed substrate divided by maximum "upwelled" concentration, (see Sect. 2.4)) are shown in Table 1 (closed system) and 2 (open system). In the case of the closed
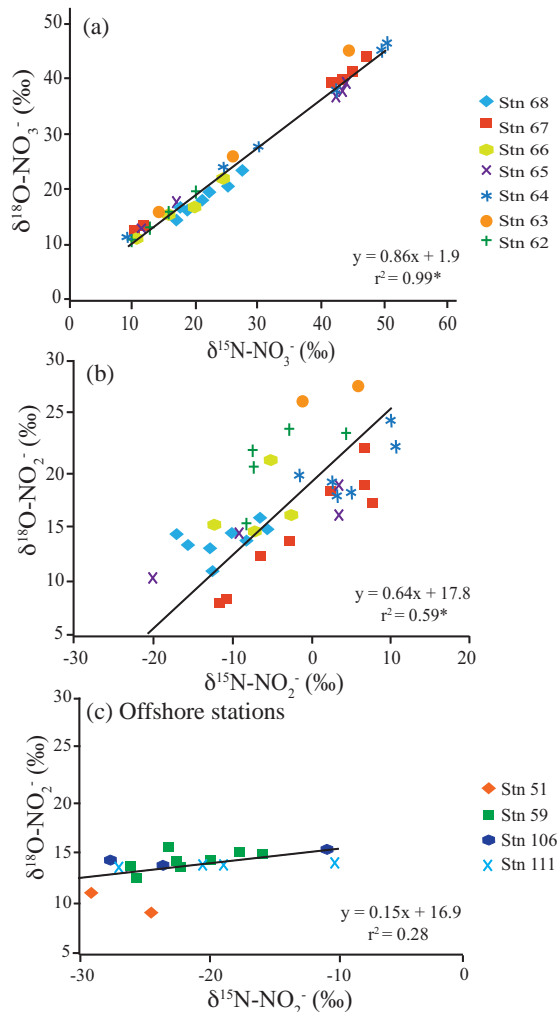
Figure 5. Relationships between $\delta^{15}N$ and $\delta^{18}O$ for NO_3^- and NO_2^-, respectively, for $O_2 \leq 10\,\mu M$. **(a)** $\delta^{18}O$-NO_3^- vs. $\delta^{15}N$-NO_3^- for station 62 to 68. **(b)** $\delta^{18}O$-NO_2^- vs. $\delta^{15}N$-NO_2^- for station 62 to 68. **(c)** $\delta^{18}O$-NO_2^- vs. $\delta^{15}N$-NO_2^- for M90 offshore stations 51, 59, 106 and 111 (see text, Sect. 3.3). For each plot, overall linear regressions are shown. Significant correlation coefficients at a 0.05 significance level are denoted by *.

Table 1. ε for NO_3^- reduction and net N loss estimated from both DIN consumption and produced biogenic N_2 using Rayleigh closed system equations (Eqs. 1–3). Results are calculated for f based on either $Np_{expected}$ (Eqs. 7–9), biogenic N_2 (Eqs. 12–14) and measured substrate divided by maximum (upwelled) substrate concentrations (see text, Sect. 2.4). The standard error of the slope (ε) is shown.

	Basis for f	ε	y intercept	r^2
$\delta^{15}N$-NO_3^-	$Np_{expected}$	13.9 ± 0.7	3.74	0.92
	N_2 Biogenic	14.3 ± 0.9	3.71	0.95
	$[NO_3^-]/[NO_3^-]_{max}$	14.7 ± 0.6	-0.55	0.95
$\delta^{15}N$-DIN	$Np_{expected}$	6.3 ± 0.3	7.20	0.92
	N_2 Biogenic	6.6 ± 0.4	6.71	0.94
	DIN/DIN_{max}	7.4 ± 0.6	10.90	0.91
$\delta^{15}N$-Biogenic N_2	$Np_{expected}$	10.5 ± 1.5	2.94	0.70
	N_2 Biogenic	10.6 ± 1.5	3.04	0.72

is more realistic based on prior isotopic measurements for source waters (e.g., Bourbonnais et al., 2015).

4 Discussion

4.1 Behavior of NO_2^-

NO_2^- is an important intermediate during either oxidative or reductive N-cycle pathways and can accumulate at relatively high concentrations through the ocean. While NO_2^- is generally elevated at the base of the sunlit euphotic zone (i.e. primary NO_2^- maximum; Dore and Karl, 1996; Lomas and Lipschultz, 2006), highest concentrations are found in ODZ's as part of the secondary NO_2^- maximum (Codispoti and Christensen 1985; Lam et al., 2011). Accordingly, high NO_2^- concentrations ranging from 7.2 to 10.7 μM were observed at 50–75 m depth in coastal O_2-depleted waters in this study as a likely consequence of dissimilatory NO_3^- reduction (e.g., Lipschultz et al., 1990; Lam et al., 2009; Kalvelage et al., 2013).

To assess the influence of the various N cycle processes that have NO_2^- as either a substrate or product, we first examined the relationship between the $\delta^{15}N$ and $\delta^{18}O$ of NO_2^-. Several processes can influence the isotopic composition of NO_2^-. NO_3^- reduction to NO_2^- is associated with a ε of 20 to 30 ‰ (Cline and Kaplan, 1975; Brandes et al., 1998; Voss et al., 2001; Granger et al., 2004, 2008) and acts to produce NO_2^- depleted in ^{15}N and ^{18}O. In contrast, NO_2^- reduction as part of either anammox, denitrification or DNRA increases both the $\delta^{15}N$ and $\delta^{18}O$ of residual NO_2^-, with laboratory and field estimates for ε clustering around 12 to 16 ‰ (Bryan et al., 1983; Brunner et al., 2013; Bourbonnais et al., 2015). However, NO_2^- oxidation to NO_3^- at low or non-detectable O_2 has been shown to be an important sink for NO_2^- in ODZs (e.g. Füssel et al., 2012). Anammox bacteria can also use
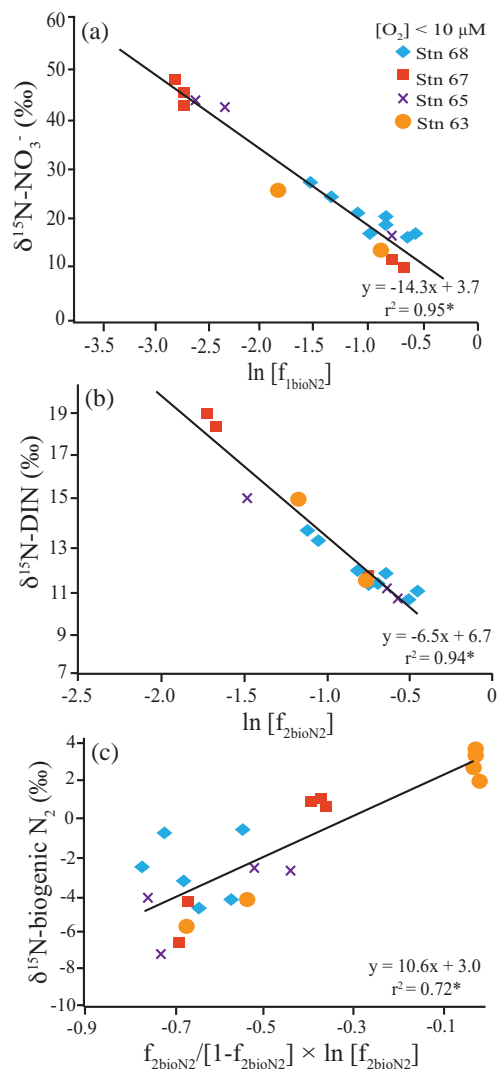
system, ε values were in all cases lower than canonical ones, ranging narrowly from ~ 6 ‰ for changes in the $\delta^{15}N$ of DIN to ~ 14 ‰ for changes in $\delta^{15}N$-NO_3^- (Table 1). For the open system equations, estimated ε was higher and covered a large and unrealistic range from ~ 12 ‰ for changes in the biogenic N_2 to ~ 63 ‰ for changes in the $\delta^{15}N$ of NO_3^-. For our inshore water stations, where we observed a single water mass (Fig. 2), a closed system should be a more realistic approximation of ε. The Rayleigh equations' y intercepts, where $f = 1$, represent the initial $\delta^{15}N$ of NO_3^- or DIN, and varied from -0.5 to 10.9 and -21.9 to 8.5 ‰ for closed and open systems, respectively. The higher end of this range

Figure 6. Raleigh relationships used to estimate ε (slope) and initial δ^{15}N-substrate (y intercept) assuming a closed system. **(a)** for NO_3^- reduction (Eq. 1 and text, Sect. 2.4), **(b)** for N-loss calculated from the substrate (DIN) consumption (Eq. 2 and text, Sect. 2.4) and **(c)** for N-loss calculated from the δ^{15}N of biogenic N_2 (Eq. 3 and text, Sect. 2.4). In **(c)**, only samples with O_2 concentrations less than $10\,\mu M$ and biogenic N_2 values $> 7.5\,\mu M$ were considered. Significant correlation coefficients at a 0.05 significance level are denoted by *.

Figure 7. N deficit, biogenic N in N_2 and δ^{15}N-N_2 anomaly with O_2 overlaid. **(a)** N deficit calculated using PO_4^{3-} (μM) (Np_{def}) and assuming Redfield stoichiometry (see Eqs. 9, 10 and 11, Sect. 2.4). **(b)** biogenic N in N_2 (μM). **(c)** δ^{15}N-N_2 anomaly relative to equilibrium with atmosphere (‰). Biogenic N_2 or δ^{15}N-N_2 anomaly were not measured at stations 62, 64 and 66.

NO_2^- as an electron donor during CO_2 fixation under anaerobic conditions (Strous et al., 2006).

Nitrite oxidation has its own unique set of isotope effects (Casciotti, 2009; Buchwald and Casciotti, 2010). Nitrite oxidation incurs an unusual inverse N isotope effect varying from -13 ‰ for aerobic (Casciotti, 2009) to -30 ‰ for anammox-mediated NO_2^- oxidation (Brunner et al., 2013), resulting in lower δ^{15}N for NO_2^- as it is oxidized to NO_3^-, and increasing $\Delta\delta^{15}$N. Moreover, enzyme catalysis associated with NO_2^- oxidation is readily reversible (Friedman et
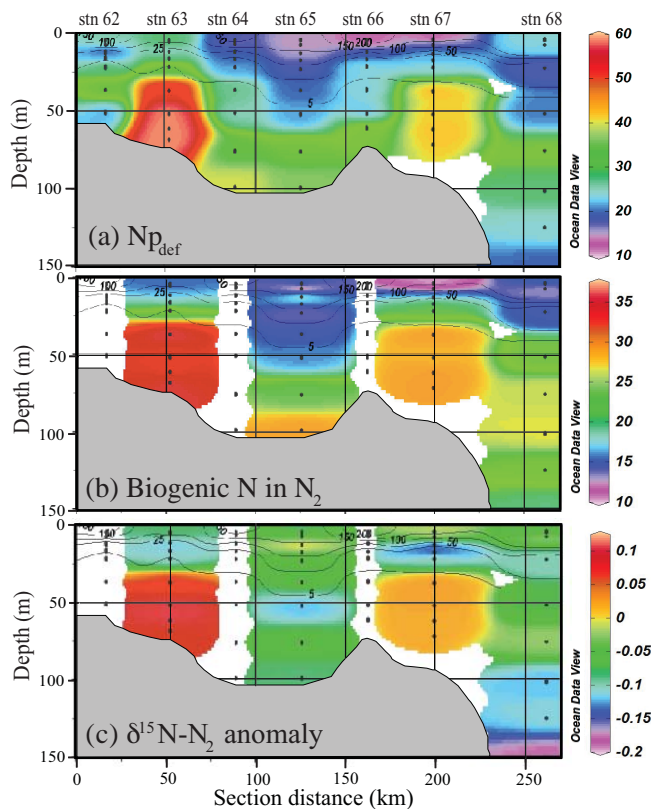
al., 1986) also causing O isotope exchange between NO_2^- and water (Casciotti et al., 2007). O atom incorporation during both NH_4^+ and NO_2^- oxidation have also been shown to occur with significant isotope effect, such that the δ^{18}O of newly microbially produced NO_3^- in the ocean range from -1.5 to 1.3 ‰ (Buchwald and Casciotti, 2012).

Past studies have found NO_2^- δ^{18}O values in ODZ's in isotope equilibrium with water as a likely consequence of relatively long turnover time (e.g., Buchwald and Casciotti, 2013; Bourbonnais et al., 2015). O isotope exchange involves the protonated form, HNO_2, but because of its high pKa as compared to NO_3^-, this process can occur even at neutral to alkaline ocean pH on a timescale of 2 to 3 months at environmentally relevant temperatures (Casciotti et al., 2007). NO_2^- δ^{18}O isotopic composition at equilibrium with water is a function of the δ^{18}O of water and temperature ($+14$ ‰ for seawater at $22\,°C$) (Casciotti et al., 2007; Buchwald and Casciotti, 2013) and is independent of its δ^{15}N value such that plots of NO_2^- δ^{18}O vs. δ^{15}N usually have a slope of near zero. This is seen in our NO_2^- data from offshore stations occupied during M90 (Fig. 5c).

We observed, for the first time, a significant linear relationship for $NO_2^- \delta^{18}O$ vs. $\delta^{15}N$ at our inshore stations (slope $= 0.64 \pm 0.07$, $r^2 = 0.59$, p value $= 3 \times 10^{-6}$) where $O_2 < 10 \mu M$ (Fig. 5b). Coupled $\delta^{15}N$ and $\delta^{18}O$ effects for NO_2^- have not been as well studied as NO_3^-. Nevertheless, if NO_2^- turnover was faster than equilibration time with water, NO_3^- and NO_2^- reduction whether as part of the denitrification, anammox or DNRA pathways, should also produce a positive relationship between $NO_2^- \delta^{15}N$ and $\delta^{18}O$. In contrast to our offshore stations (Fig. 5c), this positive relationship thus demonstrates that the oxygen isotopic composition of NO_2^- is not in equilibrium with water due to both rapid NO_2^- turnover and the dominance of NO_2^- reduction over oxidation in Peru coastal waters. Higher rates for aerobic NH_4^+ and NO_2^- oxidation, as well as anaerobic NO_3^- reduction to NO_2^-, and further reduction to NH_4^+ (DNRA) or N_2, have been reported in shallow waters off Peru presumably due to increased coastal primary production and organic matter supply to the in-shore OMZ (e.g. Codispoti et al., 1986; Lam et al., 2011; Kalvelage et al., 2013). However, as our observations are restricted to anoxic waters, only high rates of N-loss could explain this more rapid NO_2^- turnover.

In principal, we can estimate NO_2^- turnover time from knowledge of rates for exchange with water and assumptions of the $\delta^{18}O$ vs. $\delta^{15}N$ slope expected in the absence of exchange. Unfortunately, the slope of the relationship between $NO_2^- \delta^{18}O$ vs. $\delta^{15}N$ expected in the absence of equilibration with water is not yet known. An upper limit for turnover time for NO_2^- can be estimated based on equilibration time as a function of in situ pH and temperature (Buchwald and Casciotti, 2013). During the M91 cruise in December, subsurface temperature was 13 to 15 °C along our transect and corresponding pH was near 7.8 (Michelle Graco, unpublished data). Assuming the NO_2^- pool is in steady-state, we estimated an equilibration time of up to ~ 40 days for pH near 7.8 (estimated from equation 1 and Fig. 2 in Buchwald and Casciotti, 2013). A turnover time of up to 40 days implies a flux of N through the NO_2^- pool of at least $0.21 \mu M d^{-1}$, as estimated from the maximum NO_2^- concentration observed in this study divided by this estimated turnover time. Assuming steady-state, this range also approximates the rates of NO_3^- reduction as well as NO_2^- oxidation plus production of N_2 from NO_2^-. This estimated flux is consistent with measured high NO_3^- reduction and NO_2^- oxidation rates of up to $\sim 1 \mu M d^{-1}$ in Peru coastal waters (< 600 m depth, Kalvelage et al., 2013).

NO_2^- oxidation is a chemoautotrophic process that requires a thermodynamically favorable electron acceptor such as O_2. As mentioned above, NO_2^- oxidation appears to occur in ODZ's at low or non-detectable O_2 (e.g. Füssel et al., 2012) despite lack of knowledge of its thermodynamically favorable redox couple. The difference in $\delta^{15}N$ between NO_2^- and NO_3^- ($\Delta\delta^{15}N = \delta^{15}N\text{-}NO_3^- - \delta^{15}N\text{-}NO_2^-$

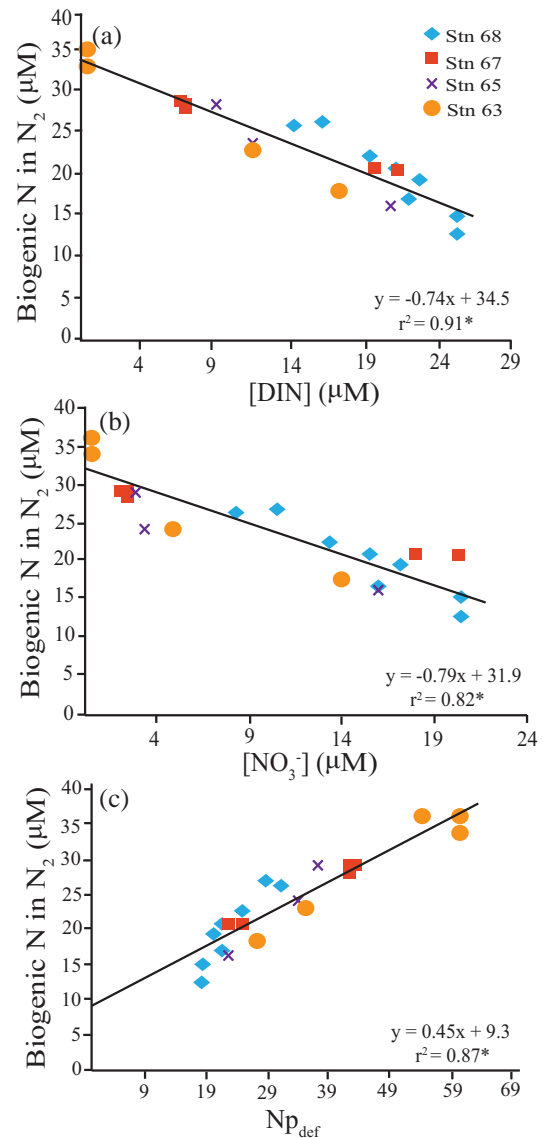**Figure 8.** Cross-plots of biogenic N in N_2 vs. DIN **(a)**, NO_3^- **(b)** and Np_{def} **(c)**, see Eqs. (9–11) in text. All plots have the overall linear regression overlaid. All the points are restricted to O_2 concentrations less than $10 \mu M$. Biogenic N_2 was not measured for stations 62, 64 and 66. Significant correlation coefficients at a 0.05 significance level are denoted by *.

see Sect. 3.3) is further evidence for the presence of NO_2^- oxidation in the ODZ (e.g. Casciotti et al., 2013). At steady-state, and in the absence of NO_2^- oxidation, $\Delta\delta^{15}N$ should be no more than the ε for NO_3^- reduction (20 to 30 ‰) minus the ε for NO_2^- reduction by denitrifying or anammox bacteria (12–16 ‰; Bryan et al., 1983; Brunner et al., 2013; Bourbonnais et al., 2015) or 8–18 ‰ . Our results range from 15–40 ‰ and average 29.8 ‰ for samples with O_2 concentrations $< 10 \mu M$.

The inverse kinetic isotope effect associated with NO_2^- oxidation is likely responsible for these high $\Delta\delta^{15}N$ values (e.g. Casciotti and Buchwald, 2012; Casciotti et al., 2013). Taking all isotope effects into account, the following equation can be derived to estimate $\Delta\delta^{15}N$ at steady-state:

$$\Delta\delta^{15}N(\text{steady state}) = \varepsilon_{NO_3-red} - (1-\gamma) \qquad (15)$$
$$\times \varepsilon_{NO_2-red} - \gamma \times \varepsilon_{NO_2-oxid},$$

where γ is the fraction of NO_2^- oxidized back to NO_3^-. Highest values (over 30 ‰) are found between 50 and 100 m, implying greater importance for NO_2^- oxidation in deeper waters.

Given that ε_{NO_2-oxid} has been reported to be -13 ‰ for aerobic NO_2^- oxidation and using the literature ranges for ε_{NO_3-red} and ε_{NO_2-red} above, our observed $\Delta\delta^{15}N$ implies that up to 100 % of NO_2^- produced by NO_3^- reduction could be oxidized back to NO_3^-. This estimate is higher than ratios of NO_2^- oxidation / NO_3^- reduction of up to 54 % for the Peruvian coastal ODZ derived from direct rate measurements (Lam et al., 2009; Kalvelage et al., 2013), and should thus be considered as an upper limit. Alternatively, NO_2^- oxidation also occurs as part of the overall metabolism of anammox bacteria (Strous et al., 2006) which can be the dominant N_2 producers in the Peru ODZ (Kalvelage et al., 2013). A large inverse kinetic ε for NO_2^- oxidation of ~ -30 ‰ has been observed for anammox bacteria in culture (Brunner et al., 2013). If this is the sole pathway for NO_2^- oxidation, our data suggest NO_2^- oxidation up to only ~ 80 % of total NO_3^- reduction. However, anammox bacteria only oxidize a minor fraction of NO_2^- to NO_3^- in culture. At the same time, estimates of NO_2^- oxidation (8.48 to 928 nM d^{-1}) are significantly higher than N-loss rates by anammox (2.84 to 227 nmol N L^{-1} d^{-1}) on the Peruvian shelf (Kalvelage et al., 2013), clearly indicating non-anammox related nitrite oxidation.

The deviations from a 1 : 1 relationship for $NO_3^-\delta^{18}O$ and $\delta^{15}N$ can also be indicative of NO_2^- oxidation. During NO_3^- uptake or dissimilative NO_3^- reduction, $NO_3^-\delta^{15}N$ and $\delta^{18}O$ increase equally with a ratio of 1:1 (Granger et al., 2004, 2008). We observed a slope of about 0.86 (Fig. 5a) for the $NO_3^-\delta^{18}O$ vs. $\delta^{15}N$ relationship in the in-shore Peru ODZ, similar to recent off-shore observations (Bourbonnais et al., 2015). Prior reports of deviations toward higher values for the slope were indicative of addition of newly nitrified NO_3^- from a relatively low $\delta^{15}N$ source (e.g. see Sigman et al., 2005; Bourbonnais et al., 2009). Our observed deviation toward slopes < 1 can instead be explained by the addition of newly nitrified NO_3^- with a lower $\delta^{18}O$-NO_3^-, mostly derived from water (Andersson and Hooper, 1983), relative to the high ambient $\delta^{18}O$-NO_3^- values. In fact, a slope for $\delta^{18}O : \delta^{15}N$ of either greater or less than 1 can be observed, depending on initial environmental NO_3^- isotopic composition relative to any in situ sources (Casciotti

et al., 2013). Casciotti and Buchwald (2012) showed model results where NO_2^- oxidation generally produces a slope < 1 for the $NO_3^-\delta^{18}O$ vs. $\delta^{15}N$ relationship, when the $NO_3^-\delta^{15}N$ and $\delta^{18}O$ are higher than ~ 15 ‰ as observed in Casciotti et al. (2013) and Bourbonnais et al. (2015).

4.2 Isotope effects for N-loss

As described above, the Rayleigh fractionation equations (Eqs. 1 to 6) are used here to estimate ε values (Mariotti et al., 1981; Altabet, 2005) and examine the significance of calculations using (a) different approaches for calculating f (Eqs. 7 and 14), (b) changes in the $\delta^{15}N$ of substrate (DIN) vs. changes in the $\delta^{15}N$ of product, and (c) closed vs. open system equations. This approach provides redundancy in our estimates of ε and tests implied assumptions including N and ^{15}N balance between NO_3^- or DIN loss and the accumulation of biogenic N_2.

Linear regression coefficients for ε calculated using the different approaches presented in Sect. 2.4 are listed in Tables 1 and 2. For example, Rayleigh closed system plots for $\delta^{15}N$-NO_3^-, $\delta^{15}N$-DIN, or $\delta^{15}N$ biogenic N_2 as a function of f_{2bioN_2} are shown in Fig. 6. Surprisingly, ε values estimated from the slope of these relationships are not sensitive to choice of method for calculating f despite the lack of 1 : 1 correspondence between different bases ($Np_{expected}$, biogenic N_2, or $[NO_3^-] / [NO_3^-]_{max}$). In the case of ε calculated from changes in $\delta^{15}N$-DIN, ε ranged narrowly with choice of f from 6.3 to 7.4 ‰ with standard errors on the slope of < 0.6 ‰ (Table 1). As there was no significant difference between bases for calculating f, it appears that all three of our approaches are valid for this purpose.

However, ε for N-loss (closed system) does vary significantly between calculations using changes in $\delta^{15}N$-NO_3^-, $\delta^{15}N$-DIN, or $\delta^{15}N$ biogenic N_2. ε is largest for changes in $\delta^{15}N$-NO_3^- (~ 14 ‰) and smallest for changes in $\delta^{15}N$-DIN (~ 7 ‰). ε based on $\delta^{15}N$ biogenic N_2 is intermediate (~ 11 ‰). The latter two, using DIN or biogenic N_2 as the basis to calculate ε, are more representative of N-loss. Calculations based on changes in $\delta^{15}N$-NO_3^- are affected by NO_2^- accumulation and isotope effects of NO_2^- oxidation (see above). The 4 ‰ difference in ε calculated from changes in $\delta^{15}N$ of biogenic N_2 vs. $\delta^{15}N$ of DIN may arise from the contribution of NH_4^+ derived from organic matter to biogenic N_2 via the anammox process. Supporting this hypothesis, NH_4^+ accumulation (5.3–7.5 µM) associated with a relatively low $\delta^{15}N$-NH_4^+ of 3.8 to 6.1 ‰ was observed at 125 and 200 m bottom water depths at shallow stations located in the studied area ($\sim 12.3°$ S and 77.3° W) in January 2013 (unpublished results). A contribution of NH_4^+ from organic material and consumption by anammox could therefore supply comparatively lower $\delta^{15}N$ to the biogenic N_2 pool, increasing ε.

Table 2. ε for NO_3^- reduction, and net N loss estimated from both DIN consumption and produced biogenic N_2 using Rayleigh open system equations (Eqs. 4–6). Results are calculated for f based on either $Np_{expected}$ (Eqs. 7–9), biogenic N_2 (Eqs. 12–14), and measured substrate divided by maximum (upwelled) substrate concentrations (see text, Sect. 2.4). The standard error of the slope (ε) is shown.

	Basis for f	ε	y intercept	r^2
δ^{15}N-NO_3^-	$Np_{expected}$	63.0 ± 4.5	-18.42	0.86
	N_2 Biogenic	66.30 ± 6.2	-21.92	0.87
	$[NO_3^-] / [NO_3^-]_{max}$	38.9 ± 2.7	6.19	0.87
	$Np_{expected}$	17.4 ± 1.2	3.26	0.88
δ^{15}N-DIN	N_2 Biogenic	20.0 ± 1.8	1.72	0.89
	DIN / DIN_{max}	13.2 ± 0.9	8.45	0.91
δ^{15}N-Biogenic N_2	$Np_{expected}$	12.3 ± 1.9	1.94	0.67
	N_2 Biogenic	14.15 ± 2.1	2.25	0.68

The different approaches for estimating the ε for N-loss can also be evaluated by examining the initial substrate δ^{15}N predicted where $f = 1$ for each set of regressions. In the case of changes in δ^{15}N-DIN and using $Np_{expected}$ or biogenic N_2 as bases for f, realistic values are found consistent with the source of upwelled waters of 6 to 7 ‰ (Table 1; also see Ryabenko et al., 2012). For regressions based on changes in δ^{15}N-biogenic N_2, initial δ^{15}N values are somewhat lower (~ 3 ‰), possibly due to a source from organic N decomposition.

Estimates of ε using open-system equations are generally much higher than for closed system equations particularly for changes in δ^{15}N-NO_3^- with unrealistically high values (39–63 ‰; Table 2). However, values for both closed and open systems tended to converge for estimates based on changes in δ^{15}N-DIN or δ^{15}N-biogenic N_2 with the latter having no significant difference. Estimates of substrate initial δ^{15}N using the open system equations range widely and do not consistently reflect realistic values (Table 2).

Closed system estimates of ε are likely more reliable in our setting because of low likelihood of mixing between water masses of contrasting characteristics on the shelf. Temperature and salinity in the ODZ at our stations narrowly ranged from 13.5 to 15 °C and 34.88 to 34.98 (Fig. 2), similar to T/S signatures from offshore source waters (Bourbonnais et al., 2015), and suggestive of a single water mass. Accordingly, as in Bourbonnais et al. (2015), we view the closed system equations as most reliable with a value of ~ 6.5 ‰ for ε based on changes in δ^{15}N DIN as the likely best estimate. However, given the overlap with the results of open system equations for changes in δ^{15}N of biogenic N_2, an upper bound of ~ 11 ‰ appears appropriate. This range in ε for N-loss falls below the results of Bourbonnais et al. (2015) for a near-coastal eddy in the same region and time period (~ 14 ‰) and is much less than the canonical range of 20 to 30 ‰ (Brandes et al., 1998; Voss et al., 2001; Granger et al., 2008). As discussed in Bourbonnais et al. (2015), a lower overall ε for net N-loss could help resolve any imbalance in the oceanic N-budget, by decreasing the ratio of sedimentary and water-column N-loss necessary to account for the observed δ^{15}N of mean ocean NO_3^-.

There are several reasonable explanations for these relatively low ε values in coastal waters. These include higher microbial growth rates associated with higher productivity, which would shift biochemical rate limitation away from enzyme reactions to membrane transport with low fractionation potential (e.g. Wada and Hattori, 1978). Another is greater influence from benthic N cycling processes in our relatively shallow inshore system as compared to deeper waters. Sediment N-loss has been shown to incur low ε due to, in analogous fashion to the affect of microbial growth rate, dominance of substrate transport limitation through the sediment (Brandes and Devol, 1997). This possibility will be explored further in the next section. Unlikely explanations for our relatively low ε values for N-loss include the effects of decreasing NO_3^- concentration (Kritee et al., 2012) and contributions from organic N via anammox to biogenic N_2. Lack of curvature in the Rayleigh plots demonstrates a lack of dependence of substrate concentration (Fig. 6a, b) as the range in f corresponds to a large range in NO_3^- or DIN concentrations. The possible effects of contributions from organic N to biogenic N_2 has already been taken into account in calculations based on changes in the δ^{15}N of biogenic N_2, as discussed above.

4.3 Using ε values for estimating sediment N-loss

The low ε value we observe for water column N-loss at our inshore stations may be explained by contributions from sediment N-loss (e.g. see Sigman et al., 2003). If so, observed ε for N-loss in the water-column should be the weighted average of the actual ε values for N-loss in the water column and sediments:

$$\varepsilon_{obs} = \varepsilon_{wc} \times (1 - P_{sed}) + \varepsilon_{sed} \times P_{sed}, \qquad (16)$$

where ε_{wc} and ε_{sed} are the isotope effect of water column and sediments and P_{sed} is the proportion of water column and sedimentary N-loss, respectively. We take 6.8 ± 0.5 ‰ as the value for ε_{obs} (Fig. 6, Table 1), a value of 13.8 ± 1.3 ‰ for ε_{wc} as estimated for offshore waters by Bourbonnais et al. (2015), and a ε_{sed} of 1.5 ‰ as in Sigman et al. (2003). From these numbers, we estimated that the proportion of N-loss due to sedimentary N-loss could be up to ~ 60 % (48 to 64 %) at our coastal stations, which is in the same range than previously reported for other marine coastal environments, e.g. Saanich Inlet (also up to 60 %; Bourbonnais et al., 2013). Our estimate is higher than the 25 % of benthic vs. total N-loss from a reaction-diffusion model and direct flux measurements for the same coastal region off Peru (Kalvelage et al., 2013). However, our comparison to direct measurements of fluxes should be considered tentative as they are made at single locations over relatively short time periods are thus subject to considerable spatial and temporal heterogeneity.

5 Conclusions

The inshore Peru ODZ is distinguished from offshore by its high productivity as a consequence of coastal upwelling as well as possible greater influence from benthic processes. To examine impact on N-loss processes and their isotope effects, we investigated the dynamics of N and O isotope of NO_2^- and NO_3^- at six coastal stations off Peru.

We found that N-loss representing the net effect of partial denitrification, anammox, and nitrification produced, in sum, large variations in isotopic composition. $NO_2^- \delta^{15}N$ ranged from -20 to $10\,‰$ and $NO_3^- \delta^{15}N$ ranged from 10 to $50\,‰$. Generally, NO_3^- and NO_2^- isotope values varied inversely with their concentrations as expected for Rayleigh-like fractionation effects. Isotope values were usually higher in low-O_2 near bottom waters where N species concentrations were also relatively low.

We observed, for the first time, a positive linear relationship between $NO_2^- \delta^{15}N$ and $\delta^{18}O$ at our inshore stations. In offshore ODZ waters, such a relationship has never previously been observed as $NO_2^- \delta^{18}O$ reflected equilibration with water in these regions (Buchwald and Casciotti, 2013). Our results suggest a turnover time for NO_2^- faster than the equilibration time with water and the effect of NO_2^- oxidation over NO_2^- reduction in these highly productive coastal waters. We estimated an NO_2^- turnover time of up to ~ 40 days from our data.

The difference in $\delta^{15}N$ between NO_3^- and NO_2^- ($\Delta\delta^{15}N$) was high, reaching up to $40‰$ in deeper waters, and was greater than expected from NO_3^- and NO_2^- reduction only. The influence of NO_2^- oxidation is consistent with this observation due to its inverse fractionation effect (Casciotti, 2009). Additional evidence for NO_2^- oxidation is found in the relationship between $NO_3^- \delta^{15}N$ and $\delta^{18}O$. NO_3^- reduction alone is expected to produce a $1:1$ relationship (Granger et al., 2008). While we observed a linear relationship between $NO_3^- \delta^{15}N$ and $\delta^{18}O$, the slope of 0.86 is indicative of simultaneous addition of NO_3^- with relatively low $\delta^{18}O$, also consistent with a role for NO_2^- oxidation at our coastal sites. However, a favorable thermodynamic couple for NO_2^- oxidation in the absence of O_2 in these waters remains unknown.

A number of different approaches for estimating ε for N-loss were compared including choice of N form for changes in $\delta^{15}N$ (NO_3^-, DIN, or biogenic N_2), closed vs. open system Rayleigh equations, and the basis for calculating the denominator in f ($Np_{expected}$, biogenic N_2, or maximum NO_3^-). For the latter, there was little difference in estimated ε despite discrepancies between the removal of NO_3^- and appearance of N_2 estimated from them. Observation of a single water mass ($T - S$ plot) in our coastal region as well as more realistic ranges for derived ε and initial $\delta^{15}N$ indicated that closed system assumptions were more realistic. Using closed system equations, relatively low ε values were calculated; $\sim 7‰$ for changes in the $\delta^{15}N$ of DIN and $\sim 11‰$ for changes in the $\delta^{15}N$ of biogenic N_2. As in Bourbonnais et al. (2015), ε calculated from changes in the $\delta^{15}N$ of NO_3^- alone was not representative of the ε for overall N-loss in consideration of the build up of NO_2^- with distinct $\delta^{15}N$. These estimates for ε for net N-loss are lower than recently reported for a nearby offshore eddy with intense N-loss ($\sim 14‰$; Bourbonnais et al., 2015). This lower ε may be attributed to the influence of sedimentary N-loss on the Peruvian shelf (e.g., Bohlen et al., 2011) with a highly suppressed ε on the overlying water column at our shallow stations. Given this assumption, we estimate that sedimentary N-loss (by both denitrification and anammox) could account for up to 60% of the total N-loss in in shore Peru ODZ waters.

Our results further support geographical variations in the ε of N-loss in ODZs, possibly related to the effects of varying primary productivity and microbial growth rates on the expression of ε and partitioning between water-column and sedimentary denitrification. These variations need to be considered in future global isotopic N budget (e.g. see Brandes and Devol, 2002), potentially bringing the global N budget more in balance. This is further supported by the relatively lower ε for N-loss of $\sim 14‰$ recently observed offshore in the ETSP ODZ by Bourbonnais et al. (2015). A lower water-column ε for N-loss also decreases the fraction of sedimentary denitrification needed to balance the global isotopic N budget (Brandes and Devol, 2002; Altabet, 2007).

References

Alkhatib, M., Lehmann, M. F., and del Giorgio, P. A.: The nitrogen isotope effect of benthic remineralization-nitrification-denitrification coupling in an estuarine environment, Biogeosciences, 9, 1633–1646, doi:10.5194/bg-9-1633-2012, 2012.

Altabet, M. A.: Isotopic tracers of the marine nitrogen cycle: present and past, in The handbook of environmental chemistry, vol. 2, edited by: Hutzinger, O., Springer-Verlag, Berlin, Heidelberg, 251–293, 2005.

Altabet, M. A.: Constraints on oceanic N balance/imbalance from sedimentary ^{15}N records, Biogeosciences, 4, 75–86, doi:10.5194/bg-4-75-2007, 2007.

Andersson, K. K. and Hooper, A. B.: O_2 and H_2O are each the source of one O in NO_2^- Produced from NH_3 by Nitrosomonas: ^{15}N-NMR evidence, FEBS Lett., 164, 236–240, 1983.

Babbin, A. R., Keil, R. G. Devol, A. H., and Ward, B. B.: Organic Matter Stoichiometry, Flux, and Oxygen Control Nitrogen Loss in the Ocean, Science, 344, 406–408, 2014.

Bohlen, L., Dale, A. W., Sommer, S., Mosch, T., Hensen, C., Noffke, A., Scholz, F., and Wallmann, K.: Benthic nitrogen cycling traversing the Peruvian oxygen minimum zone, Geochim. Cosmochim. Ac., 75, 6094–6111, 2011.

Bourbonnais, A., Lehmann, M. F. Waniek, J. J., and Schulz-Bull, D. E.: Nitrate Isotope Anomalies Reflect N_2 Fixation in the Azores Front Region (subtropical NE Atlantic), J. Geophys. Res.-Oceans, 114, C03003, doi:10.1029/2007JC004617, 2009.

Bourbonnais, A., Lehmann, M. F., Hamme, R. C., Manning, C. C, and Kim Juniper, S.: Nitrate elimination and regeneration as evidenced by dissolved inorganic nitrogen isotopes in Saanich Inlet, a seasonally anoxic fjord, Mar. Chem., 157, 194–207, 2013.

Bourbonnais, A., Altabet, M. A., Charoenpong, C. N., Larkum, J., Hu, H., Bange, H. W., and Stramma, L.: N-loss isotope effects in the Peru oxygen minimum zone studied using a mesoscale eddy as a natural tracer experiment, Global Biogeochem. Cy., 29, 793–811, doi:10.1002/2014GB005001, 2015.

Brandes, J. A. and Devol, A. H. Isotopic Fractionation of Oxygen and Nitrogen in Coastal Marine Sediments, Geochim. Cosmochim. Ac., 61, 1793–1801, 1997.

Brandes, J. A. and Devol, A. H.: A global marine-fixed nitrogen isotopic budget: Implications for Holocene nitrogen cycling, Global Biogeochem. Cy., 16, 67-1–67-14, 2002.

Brandes J. A., Devol, A. H., Yoshinari, T., Jayakumar D. A., and Naqvi, S. W. A.: Isotopic composition of nitrate in the central Arabian Sea and eastern tropical North Pacific: A tracer for mixing and nitrogen cycles, Limnol. Oceanogr., 43, 1680–1689, 1998.

Brunner, B. Contreras, S., Lehmann, M. F., Matantseva, O., Rollog, M., Kalvelage, T., Klockgether, G., Lavik, G., Jetten, M. S. M., Kartal, B., and Kuypers, M. M. M: Nitrogen isotope effects induced by anammox bacteria, P. Natl. Acad. Sci. USA, 110, 18994–18999, 2013.

Bryant, J. P., Chapin, F. S., and Klein, D. R. Carbon uutrient balance of boreal plants in relation to vertebrate herbivory, Oikos, 40, 357–68, 1983.

Buchwald, C. and Casciotti, K. L.: Oxygen isotopic fractionation and exchange during bacterial nitrite oxidation, Limnol. Oceanogr., 55, 1064–1074, 2010.

Buchwald, C. and Casciotti, K. L.: Isotopic ratios of nitrite as tracers of the sources and age of oceanic nitrite, Nat. Geosci., 6, 308–313, 2013.

Casciotti, K. L.: Inverse kinetic isotope fractionation during bacterial nitrite oxidation, Geochim. Cosmochim. Ac., 73, 2061–2076, 2009.

Casciotti, K. L. and Buchwald, C.: Insights on the marine microbial nitrogen cycle from isotopic approaches to nitrification, Front. Microbiol., 3, 356, doi:10.3389/fmicb.2012.00356, 2012.

Casciotti, K. L. and McIlvin, M. R.: Isotopic analyses of nitrate and nitrite from reference mixtures and application to eastern tropical North Pacific waters, Mar. Chem., 107, 184–201, 2007.

Casciotti, K. L. Sigman, D. M., Hastings, M. G., Böhlke, J. K., and Hilkert, A.: Measurement of the oxygen isotopic composition of nitrate in seawater and freshwater using the denitrifier method, Anal. Chem., 74, 4905–4912, 2002.

Casciotti, K. L., Böhlke, J. K., McIlvin, M. R.,Mroczkowski, S. J., and Hannon, J. E.: Oxygen isotopes in nitrite: analysis, calibration, and equilibration, Anal. Chem., 79, 2427–2436, 2007.

Casciotti, K. L., McIlvin, M., and Buchwald, C.: Oxygen Isotopic Exchange and Fractionation during Bacterial Ammonia Oxidation, Limnol. Oceanogr., 55, 753–762, 2010.

Casciotti, K. L., Buchwald, C., and McIlvin, M.: Implications of nitrate and nitrite isotopic measurements for the mechanisms of nitrogen cycling in the Peru oxygen deficient zone, Deep-Sea Res. Pt. I, 80, 78–93, 2013.

Chang, B. X., Devol, A. H., and Emerson, S. R.: Denitrification and the nitrogen gas excess in the eastern tropical South Pacific oxygen deficient zone, Deep-Sea Res. Pt. I, 57, 1092–1101, 2010.

Cline, J. D. and Kaplan, I. R.: Isotopic Fractionation of Dissolved Nitrate during Denitrification in the Eastern Tropical North Pacific Ocean, Mar. Chem., 3, 271–299, 1975.

Charoenpong, C. N., Bristow, L. A., and Altabet, M. A.: A continuous flow isotope ratio mass spectrometry method for high precision determination of dissolved gas ratios and isotopic composition, Limnol. Oceanogr.-Meth., 12, 323–337, 2014.

Codispoti, L. A.: An oceanic fixed nitrogen sink exceeding $400\,\mathrm{Tg\,N\,a^{-1}}$ vs the concept of homeostasis in the fixed-nitrogen inventory, Biogeosciences, 4, 233–253, doi:10.5194/bg-4-233-2007, 2007.

Codispoti, L. A. and Christensen, J. P.: Nitrification, denitrification and nitrous oxide cycling in the eastern tropical South Pacific ocean, Mar. Chem., 16, 277–300, 1985.

Codispoti, L. A., Friederich, G. E., Packard, T. T., Glover, H. E., Kelly, P. J., Spinrad, R. W., and Barber, R. T.: High Nitrite Levels off Northern Peru: A Signal of Instability in the Marine Denitrification Rate, Science, 233, 1200–1202, 1986.

Dalsgaard, T., Thamdrup, B., Farías, L., and Revsbech, N. P.: Anammox and denitrification in the oxygen minimum zone of the eastern South Pacific, Limnol. Oceanogr., 57, 1331–1346, 2012.

Dalsgaard, T., Stewart, F. J., Thamdrup, B., Brabandere, L. D., Revsbech, P., and Ulloa, O.: Oxygen at Nanomolar Levels Reversibly Suppresses Process Rates and Gene Expression in Anammox and Denitrification in the Oxygen, mBio, 5, e01966-14, doi:10.1128/mBio.01966-14, 2014.

Deutsch, C., Sarmiento, J. L., Sigman, D. M., Gruber, N., and Dunne, J. P.: Spatial coupling of nitrogen inputs and losses in the ocean, Nature, 445, 163–167, 2007.

DeVries, T., Deutsch, C., Primeau, F., Chang, B., and Devol, A.: Global rates of water-column denitrification derived from nitrogen gas measurements, Nature, 5, 547–550, 2012.

Dore, J. E. and Karl, D. M.: Nitrification in the Euphotic Zone as a Source for Nitrite, Nitrate, and Nitrous Oxide at Station ALOHA, Limnol. Oceanogr., 41, 1619–1628, 1996.

Eugster, O. and Gruber, N.: A probabilistic estimate of global marine N-fixation and denitrification, Global Biogeochem. Cy., 26, 1–15, 2012.

Friedman, S. H., Massefski, W., and Hollocher, T. C.: Catalysis of intermolecular oxygen atom transfer by nitrite dehydrogenase of Nitrobacter agilis, J. Biol. Chem., 261, 10538–10543, 1986.

Füssel, J., Lam, P., Lavik, G., Jensen, M. M., Holtappels, M., Günter, M., and Kuypers, M. M. M.: Nitrite oxidation in the Namibian oxygen minimum zone, ISME J., 6, 1200–1209, 2012.

Granger, J. and Sigman, D. M.: Removal of nitrite with sulfamic acid for nitrate N and O isotope analysis with the denitrifier method, Rapid Commun. Mass Sp., 23, 3753–3762, 2009.

Granger, J., Sigman, D. M., Needoba, J. A., and Harrison, P. J.: Coupled nitrogen and oxygen isotope fractionation of nitrate during assimilation by cultures of marine phytoplankton, Limnol. Oceanogr., 49, 1763–1773, 2004.

Granger, J., Sigman, D. M., Lehmann, M. F., and Tortell, P. D.: Nitrogen and oxygen isotope fractionation during dissimilatory nitrate reduction by denitrifying bacteria, Limnol. Oceanogr., 53, 2533–2545, 2008.

Großkopf, T., Mohr, W., Baustian, T., Schunck, H., Gill, D., Kuypers, M. M. M., Lavik, G., Schmitz, R. A., Wallace, D. W. R., and LaRoche, J.: Doubling of marine dinitrogen-fixation rates based on direct measurements, Nature, 488, 361–364, 2012.

Gruber, N.: The dynamics of the marine nitrogen cycle and its influence on atmospheric CO_2 variations, in: The Ocean Carbon Cycle and Climate, edited by: Follows, M. and Oguz, T., Kluwer Academic, Dordrecht, the Netherlands, 97–148, 2004.

Gruber, N.: The marine nitrogen cycle: Overview of distributions and processes, in Nitrogen in the Marine Environment, 2nd Edn., edited by: Capone, D. G., Bronk, D. A., Mulholland, M. R., and Carpenter, E. J., Elsevier, Amsterdam, 1–50, 2008.

Hamersley, M. R., Lavik, G, Woebken, D., Rattray, J. E., Lam, P., Hopmans, E. C., Damsté, J. S. S., Krüger, S., Graco, M., Gutiérrez, D., and Kuypers, M. M. M.: Anaerobic ammonium oxidation in the Peruvian oxygen minimum zone, Limnol. Oceanogr., 52, 923–933, 2007.

Kalvelage, T., Jensen, M. M., Contreras, S., Revsbech, N. P., Lam, P., Günter, M., LaRoche, J., Lavik, G., and Kuypers, M. M. M.: Oxygen sensitivity of anammox and coupled N-cycle processes in oxygen minimum zones, Plos ONE, 6, e29299, doi:10.1371/journal.pone.0029299, 2011.

Kalvelage, T., Lavik, G., Lam, P., Contreras, S., Arteaga, L., Loscher, C. R., Oschlies, A., Paulmier, A., Stramma, L., and Kuypers, M. M. M.: Nitrogen Cycling Driven by Organic Matter Export in the South Pacific Oxygen Minimum Zone, Nat. Geosci., 6, 228–234, 2013.

Kritee K., Sigman, D. M., Granger, J., Ward, B. B., Jayakumar, A., and Deutsch, C.: Reduced isotope fractionation by denitrification under conditions relevant to the ocean, Geochim. Cosmochim. Ac., 92, 243–259, 2012.

Kuypers M. M., Lavik, G., Woebken, D., Schmid, M., Fuchs, B. M., Amann, R., Jørgensen, B. B., and Jetten, M. S. M.: Massive nitrogen loss from the Benguela upwelling system through anaerobic ammonium oxidation, P. Natl. Acad. Sci. USA, 102, 6478–6483, 2005.

Kuypers, M. M. M., Sliekers, A. O., Lavik, G., Schmid, M., Jørgensen, B. B., Kuenen, J. G., Sinninghe Damsté, J. S., Strous, M., and Jetten, M. S. M.: Anaerobic ammonium oxidation by anammox bacteria in the Black Sea, Nature, 422, 608–611, 2003.

Lam, P. and Kuypers, M. M. M.: Microbial nitrogen cycling processes in oxygen minimum zones, Annual Review of Marine Science, 3, 317–345, 2011.

Lam, P., Lavik, G., Jensen, M. M., van de Vossenberg, J., Schmid, M., Woebken, D., Gutiérrez, D., Amann, R., Jetten, M. S. M., and Kuypers, M. M. M.: Revising the Nitrogen Cycle in the Peruvian Oxygen Minimum Zone, P. Natl. Acad. Sci. USA, 106, 4752–4757, 2009.

Lam, P., Jensen, M. M., Kock, A., Lettmann, K. A., Plancherel, Y., Lavik, G., Bange, H. W., and Kuypers, M. M. M.: Origin and fate of the secondary nitrite maximum in the Arabian Sea, Biogeosciences, 8, 1565–1577, doi:10.5194/bg-8-1565-2011, 2011.

Lehmann, M. F., Sigman, D. M., McCorkle, D. C., Granger, J., Hoffmann, S., Cane, G., and Brunelle, B. G.: The Distribution of Nitrate $^{15}N/^{14}N$ in Marine Sediments and the Impact of Benthic Nitrogen Loss on the Isotopic Composition of Oceanic Nitrate, Geochim. Cosmochim. Ac., 71, 5384–5404, 2007.

Lipschultz, F., Wofsy, S. C., Ward, B. B., Codispoti, L. A., Friedrich, G., and Elkins, J. W.: Bacterial transformations of inorganic nitrogen in the oxygen-deficient waters of the eastern tropical South Pacific Ocean, Deep-Sea Res., 37, 1513–1541, 1990.

Liu, K. K.: Geochemistry of inorganic nitrogen compounds in two marine environments: The Santa Barbara Basin and the ocean off of Peru, PhD thesis, University of California, Los Angeles, 1979.

Lomas, M. W. and Lipschultz, F.: Forming the primary nitrite maximum: Nitrifiers or phytoplankton?, Limnol. Oceanogr., 51, 2453–2467, 2006.

Mariotti, A., Germon, J. C., Hubert, P., Kaiser, P., Letolle, R., Tardieux, A., and Tardieux, P.: Experimental determination of nitrogen kinetic isotope fractionation: Some principles; illustration for the denitrification and nitrification processes, Plant Soil, 62, 413–430, 1981.

McIlvin, M. R. and Altabet, M. A.: Chemical conversion of nitrate and nitrite to nitrous oxide for nitrogen and oxygen isotopic analysis in freshwater and seawater, Anal. Chem., 77, 5589–5595, 2005.

Noffke, A., Hensen, C., Sommer, S., Scholz, F., Bohlen, L., Mosch, T., Graco, M., and Wallman, K.: Benthic iron and phosphorus fluxes across the Peruvian oxygen minimum zone, Limnol. Oceanogr., 57, 851–867, 2012.

Penven, P., Echevin, V., Pasapera, J., Colas, F., and Tam, J.: Average circulation, seasonal cycle and mesoscale dynamics in the Peru Current System: a modelling approach, J. Geophys. Res., 110, C1002110, doi:10.1029/2005JC002945, 2005.

Richards, F. A., and Benson, B. B.: Nitrogen/argon and nitrogen isotope ratios in two anaerobic environments, the Cariaco Trench in the Caribbean Sea and Dramsfjord, Norway, Deep-Sea Res., 7, 254–264, 1961.

Ryabenko, E., Kock, A., Bange, H. W., Altabet, M. A., and Wallace, D. W. R.: Contrasting biogeochemistry of nitrogen in the Atlantic and Pacific Oxygen Minimum Zones, Biogeosciences, 9, 203–215, doi:10.5194/bg-9-203-2012, 2012.

Sigman, D. M., Casciotti, K. L., Andreani, M., Barford, C., Galanter, M., and Bohlke, J. K.: A Bacterial Method for the Nitrogen Isotopic Analysis of Nitrate in Seawater and Freshwater, Anal. Chem., 73, 4145–4153, 2001.

Sigman, D. M., Robinson, R., Knapp, A. N., Van Geen, A., McCorkle, D. C., Brandes, J. A., and Thunell, R. C.: Distinguishing between water column and sedimentary denitrification in the Santa Barbara Basin using the stable isotopes of nitrate. Geochem. Geophy. Geosy., 4, 1040, doi:10.1029/2002GC000384, 2003.

Sigman, D. M., Granger, J., DiFiore, P. J., Lehmann, M. M., Ho, R., Cane, G., and Van Geen, A.: Coupled nitrogen and oxygen isotope measurements of nitrate along the eastern North Pacific margin, Global Biogeochem. Cy., 19, GB4022, doi:10.1029/2005GB002458, 2005.

Stramma, L., Bange, H. W., Czeschel, R., Lorenzo, A., and Frank, M.: On the role of mesoscale eddies for the biological productivity and biogeochemistry in the eastern tropical Pacific Ocean off Peru, Biogeosciences, 10, 7293–7306, doi:10.5194/bg-10-7293-2013, 2013.

Strous, M., Pelletier, E., Mangenot, S., Rattei, T., Lehner, A., Taylor, M. W., and Horn, M.: Deciphering the Evolution and Metabolism of an Anammox Bacterium from a Community Genome, Nature, 440, 790–794, 2006.

Ulloa, O., Canfield, D. E., DeLong, E. F., Letelier, R. M., and Stewart, F. J.: Microbial oceanography of anoxic oxygen minimum zones, P. Natl. Acad. Sci. USA, 109, 15996–16003, 2012.

Voss, M., Dippner, J. W., and Montoya, J. P.: Nitrogen Isotope Patterns in the Oxygen-Deficient Waters of the Eastern Tropical North Pacific Ocean, Deep-Sea Res. Pt. I, 48, 1905–1921, 2001.

Wada, E. and Hattori, A.: Nitrogen isotope effects in the assimilation of inorganic compounds by marine diatoms, Geomicrobiol. J., 1, 85–101, 1978.

Ward, B. B., Devol, A. H., Rich, J. J., Chang, B. X., Bulow, S. E., Naik, H., Pratihary, A., and Jayakumar, A.: Denitrification as the Dominant Nitrogen Loss Process in the Arabian Sea, Nature, 461, 78–81, 2009.